# Operational Equivalence of Self-Switching in MZI and Nonlinear Polarization Switches Based on SOAs

Sumanta Gupta, Nicola Calabretta, Marco Presi, Giampiero Contestabile, Adrian Wonfor, *Member, IEEE*, Ranjan Gangopadhyay, *Member, IEEE*, and Ernesto Ciaramella, *Member, IEEE*

***Abstract*—Numerical simulations and experiments demonstrate the equivalence of two self-switches based on semiconductor optical amplifiers, namely the nonlinear polarization switch and the Mach–Zehnder interferometer. This equivalence is highlighted by introducing a one-to-one functional similarity among the switch components. By means of a detailed study on gain and phase difference variations in both switches, we introduce a method to determine the configurations in which the switches exhibit an equivalent power transfer function. Their operational equivalence is experimentally confirmed.**

***Index Terms*—All-optical self-switching, power equalization, semiconductor optical amplifiers (SOAs).**

## I. Introduction

Semiconductor optical amplifier (SOA)-based all-optical switches are the most promising and frequently investigated devices for all-optical applications in future generation high bit rate transparent networks, owing to a number of promising features; e.g., compactness, low-power operation, and potential large scale photonic integration. Among the several schemes and devices that were proposed and studied, the SOA Mach–Zehnder interferometer (SOA–MZI) and the nonlinear polarization switch (NPS) have been exploited for a wide spectrum of applications. In particular, although the two schemes are intrinsically different, they both exhibit self-switching capabilities. Self-switched SOA–MZIs have been used successfully to accomplish a number of different tasks, such as all-optical time-domain label separation [1], reduction of patterning effects [2], and realization of a low-loss optical combiner [3]. On the other hand, the nonlinear polarization self-switch (NPS) attracted much attention in realizing functionalities for all-optical packet processing, such as seed pulse and arbitrary function generation [4], label and payload separation in variable length bursts [5], and all-optical correlators for differential phase shift keying (DPSK) signals [6].

Compared to an SOA–MZI device, the self-NPS has the disadvantage to be intrinsically polarization sensitive. This makes it unsuitable for most practical implementations. SOA–MZI's can instead be designed to be polarization insensitive [7], [8]. On the other hand, while the power splitting ratio in any SOA–MZI device is fixed at its design stage, the NPS offers the possibility to change its symmetry easily at any time by controlling the input signal polarization; this allows for higher flexibility, and can be very useful in proof-of-concept experiments.

In spite of those differences both self-switched NPS and SOA–MZI were successfully used to perform similar all-optical functions, i.e., all-optical 2R regeneration [9], [10] and all-optical power equalization [11]. This suggests common switching characteristics and some level of operational equivalence between the schemes. Hence, it is interesting to understand if this operational equivalence can be quantitatively characterized in terms of the physical characteristics of the two switches [including imbalance, biasing, input power coupling, and state of polarization (SOP)]. Such characterization would allow to realize proof-of-principle experiments using the flexible NPS switch instead of the MZI or to perform preliminary assessment for the design of "*ad hoc*" MZI switches by using the equivalent NPS. Similarities between self-switching in the NPS and SOA–MZI were also discussed in [12], but no real attempt was ever made so far to show in detail the conditions under which those devices behave equivalently.

In this paper, we first investigate the self-switching effect in both NPS and SOA–MZI, and then, we introduce a method to determine the conditions under which the two switches produce closely matched power transfer functions. The operational equivalence of the devices is also proven experimentally, comparing their power equalization capabilities in various configurations. We found that both switches can provide equalization in the same (12 dB) dynamic range and that, as predicted by numerical analysis, under proper biasing conditions, we can achieve power equalization in large dynamic ranges even with a balanced SOA–MZI device. This shows that common balanced SOA–MZI devices can be used for packet power equalization instead of *ad hoc* unbalanced devices as in [9].

This paper is organized as follows. In Section II, we review the NPS and SOA–MZI in self-switching configuration. By comparing their power transfer function, we compare common parameters and derive a one-to-one functional equivalence of their components. In Section III, we introduce the numerical SOA models that were used to simulate both the NPS and the

Manuscript received November 1, 2007; revised January 2, 2008. This work was supported in part by the Ericsson under a grant.

S. Gupta is with the FOLE Laboratory, Department of Electronics and Electrical Communication Engineering, Indian Institute of Technology-Kharagpur, Kharagpur 721302, India (e-mail: gupta.sumanta@yahoo.co.in).

R. Gangopadhyay is with the G. S. Sanyal School of Telecommunication and the Department of Electronics and Electrical Communication Engineering, Indian Institute of Technology-Kharagpur, Kharagpur 721302, India (e-mail: ranjan@ece.iitkgp.ernet.in).

N. Calabretta, M. Presi, G. Contestabile, and E. Ciaramella are with the Centro di Eccellenza per l'Ingegneria dell'Informazione e della Comunicazione (CEIIC), Scuola Superiore Sant'Anna, Pisa 56124, Italy (e-mail: nicola.calabretta@sssup.it; marco.presi@sssup.it; giampiero.contestabile@cnit.it; e.ciaramella@sssup.it).

A. Wonfor is with the Engineering Department, University of Cambridge, Cambridge CB3 0FA, U.K. (e-mail: aw300@cam.ac.uk).

Digital Object Identifier 10.1109/JSTQE.2008.916244

1077-260X/$25.00 © 2008 IEEE

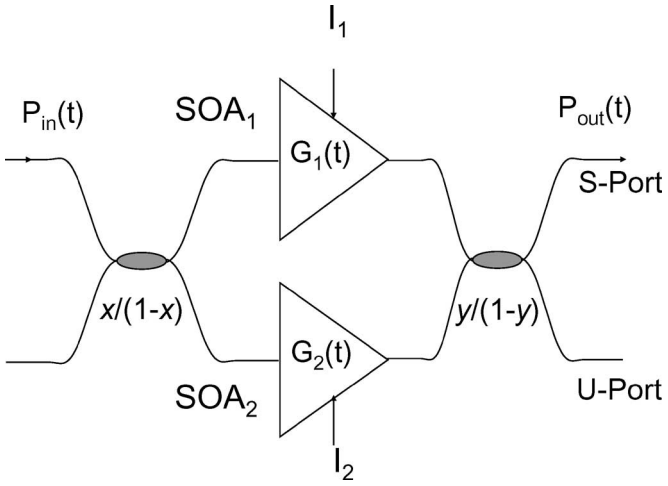


Fig. 1. Schematics of SOA–MZI-based self-switch.

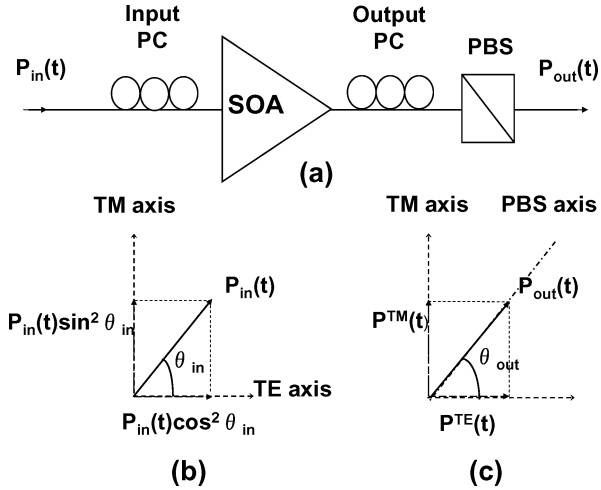


Fig. 2. (a) Self-NPS. (b) and (c) TE and TM fields distributions at the switch input and output, respectively.

SOA–MZI. In Section IV, we describe a method to determine the switch configurations producing similar transmission curves. In Section V, we present the experimental characterization of the operational equivalence of the two switches when used as all-optical power equalizers. Finally, in Section VI, we draw the conclusions.

## II. Self-Switching Principle

Fig. 1 shows the schematic of an SOA–MZI with one SOA in each arm and with input and output couplers having splitting ratios $x$ and $y$, respectively. The bias currents for the upper and lower SOAs (respectively, SOA1 and SOA2) are indicated with $I_1$ and $I_2$, respectively. The bias currents and the signal amplitude in each SOA determine the power gains ($G_1$ and $G_2$) and phase rotations [$\phi_1(t)$ and $\phi_2(t)$] experienced by the optical fields at each amplifier output. The two amplified optical fields from the two arms of the MZI interfere at the output coupler. The output power at the switched port denoted by S-port in Fig. 1 is given by

$$\begin{aligned} P_{\rm out}(t) = \{&xyG_1(t) + (1-x)(1-y)G_2(t) \\ &- 2\sqrt{xy(1-x)(1-y)G_1(t)G_2(t)} \\ &\times \cos(\Delta\phi_{\rm MZI}(t))\}P_{\rm in}(t) \end{aligned} \quad (1)$$

where $P_{\rm in}$ is the SOA–MZI input power. $\Delta\phi_{\rm MZI}$ is the total phase difference accumulated by the optical signals that is given by

$$\Delta\phi_{\rm MZI}(t) = \phi_1(t) - \phi_2(t) = -\frac{\alpha_H}{2}\ln\frac{G_1(t)}{G_2(t)} + \Delta\phi_0 \quad (2)$$

where $\alpha_H$ denotes the SOA's line-width enhancement factor [13]; $\Delta\phi_0$ is an offset phase difference contributed by the optical path difference between the interferometer arms. We note that in (1) and (2), the gain coefficients and the phase rotations are both functions of bias currents, input power $P_{\rm in}$, and input power splitting ratio, i.e., $G_i = G_i(I_i, P_{\rm in}, x)$ and $\phi_i = \phi_i(I_i, P_{\rm in}, x)$.

On the other hand, as shown in Fig. 2(a), the self-NPS is made of two polarization controllers (PCs), a polarization sensitive SOA, and a polarization beam splitter (PBS). For an input signal with power $P_{\rm in}(t)$, we can set the input PC in order to achieve linearly polarized light with a polarization angle $\theta_{\rm in}$ with respect to the SOA TE axis [see Fig. 2(b)]. The signal is then coupled into the SOA TE and TM modes having magnitude $P_{\rm in}\cos^2(\theta_{\rm in})$ and $P_{\rm in}\sin^2(\theta_{\rm in})$ respectively. These two modes experience different gains [$G_{\rm TE}(t)$ and $G_{\rm TM}(t)$] and phase rotations [$\phi_{\rm TE}(t)$ and $\phi_{\rm TM}(t)$] due to the asymmetry in carrier distributions, effective refractive index, and confinement factors. However, the TE and TM signals interplay via a common carrier reservoir as the gain saturation of each mode affects the saturation of the other. The output PC allows modification of the SOP at the SOA output to obtain a linear SOP with angle $\theta_{\rm out}$ in respect to the TE axis of the PBS [see Fig. 2(c)]. The PBS then splits $\cos^2(\theta_{\rm out})$ and $\sin^2(\theta_{\rm out})$ fractions of the amplified TE and TM optical power, respectively. In the PBS, the two field components sum up coherently, producing a kind of interference effect. After introducing $a = \cos^2(\theta_{\rm in})$ and $b = \cos^2(\theta_{\rm out})$, the output power at one of the PBS port is expressed as

$$\begin{aligned} P_{\rm out}(t) = \{&abG_{\rm TE}(t) + (1-a)(1-b)G_{\rm TM}(t) \\ &+ 2\sqrt{ab(1-a)(1-b)G_{\rm TE}(t)G_{\rm TM}(t)} \\ &\times \cos(\Delta\phi_{\rm NPS}(t))\}P_{\rm in}(t) \end{aligned} \quad (3)$$

where $\Delta\phi_{\rm NPS}$ is the nonlinear differential phase accumulated at the SOA output between TE and TM modes, and it is given by

$$\Delta\phi_{\rm NPS}(t) = \phi_{\rm TE}(t) - \phi_{\rm TM}(t) = -\frac{\alpha_H}{2}\ln\frac{G_{\rm TE}(t)}{G_{\rm TM}(t)} \quad (4)$$

with $\alpha_H$ denoting the SOA line-width enhancement factor. The nonlinear phase difference sets the output power, which is minimum when $\Delta\phi_{\rm NPS}$ is an odd multiple of $\pi$ and maximum for an even multiple.

Once the input SOP is fixed, such a phase difference can be controlled by varying the input power; due to the asymmetric gain saturation characteristic of $G_{\rm TE}(t)$ and $G_{\rm TM}(t)$, this

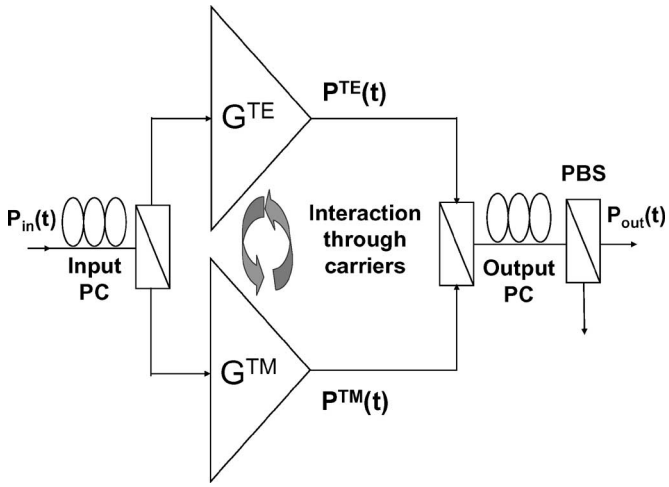


Fig. 3. Equivalence model of self-NPS.

enables the self-switching [12]. On the other hand, in the case of SOA–MZI if the SOAs have identical saturation characteristics, it is possible to obtain self-switching if the input and output couplers have different splitting ratios (and same bias currents). Indeed, in order to obtain self-switching in an SOA–MZI, it is necessary to have an imbalance of either the splitting ratios or the bias driving currents. We also note that while in the case of SOA–MZI, the minimum output power is obtained when the $\Delta\phi_{\mathrm{MZI}}$ is equal to an even multiple of $\pi$, the self-NPS results minimum output when $\Delta\phi_{\mathrm{NPS}}$ is an odd multiple of $\pi$. By comparing the transfer functions of the SOA–MZI and NPS at the selected output ports (1) and (3), we can note that the parameters $x$ and $y$ in (1) play a similar role to $a$ and $b$ in (3). This shows a functional equivalence of input/output couplers of the SOA–MZI and the input/output PCs in NPS, respectively. Furthermore, by comparing (1)–(4), we see that the same role of TE and TM gains in the NPS is played by the gains of the two SOAs in the SOA–MZI. This allows us to introduce an equivalent interferometric configuration of the NPS, like the SOA–MZI, as shown in Fig. 3. Our equivalent structure represents a one-to-one mapping between the components of the SOA–MZI and NPS: the input PC is mapped to the SOA–MZI input splitter; the output PC combined with PBS performs the same function of the SOA–MZI output coupler. The two propagation modes are represented by means of two different optical paths with a gain medium. By looking at (1) and (3), we can map $G_1$ to $G^{\mathrm{TE}}$ and $G_2$ to $G^{\mathrm{TM}}$. However, in this equivalent structure, the gain media are coupled through the carrier dynamics of the NPS. This is not the case of the SOA–MZI device, where the two amplifiers are considered to be independent. This gain coupling cannot allow the functional equivalence to be extended directly to the operational equivalence. It could be expected that if the NPS is operated in a weak coupling regime (i.e., at low input powers so that $G^{\mathrm{TE}}$ and $G^{\mathrm{TM}}$ saturate independently), the two switching characteristics of SOA–MZI and NPS would be very close. However, we will show that it is also possible to find regimes of operation in which the gains are strongly coupled but we can still obtain an operational equivalence of the switches. We will then introduce a method to achieve appropriate input and output signal SOP, coupling ratios, and bias currents to achieve those operating conditions. This will be reported in detail in Section IV.

TABLE I
SOA PARAMETERS USED IN SOA–MZI SIMULATIONS

| Parameter | Value |
|---|---|
| Active Volume | $800 \times 1.6 \times 0.2\ \mu m^3$ |
| Confinement Factor | 0.3 |
| Linewidth Enhancement Factor | 4 |
| Carrier Lifetime | 500 ps |
| Material Gain Coefficient | $2.75 \times 10^{-20}\ m^2$ |
| Carrier Density at Transparency | $10^{24}\ m^{-3}$ |
| Group Velocity | $10^8$ m/s |
| Loss in Active Layer | $2700\ m^{-1}$ |
| Nonlinear Gain Compression Factor | $4.5 \times 10^{-23}\ m^3$ |

## III. SOA MODEL

We modeled the SOA–MZI assuming that polarization insensitive bulk SOAs are used in its arms. The active length of the amplifier is divided into equal subsections with $200\,\mu\mathrm{m}$ length in a similar way to [14]. Amplified spontaneous emission (ASE) noise contribution in each subsection is realized by slicing the noise spectrum (distributed from 1450 to 1650 nm) into 20 equal bandwidth (BW) bins. In our simulations, the signal is treated as a field with a complex envelope and the ASE noise as power similar to [14]–[16]. For the chosen subsection length, homogeneously distributed bias current, and with constant envelope signal the model results less than $2\%$ error of the calculated signal and the ASE power at the SOA output compared to a case with a very small subsection length ($<20\ \mu$m). We assume a linear relationship between carrier density and material gain within each subsection, represented by

$$g_j(t) = a_0(N_j(t) - N_0) \tag{5}$$

where $a_0$, $N_j$, and $N_0$ are the differential gain coefficient, carrier density in $j$th subsection, and carrier density at transparency, respectively. The power gain $G_j(t)$ inside each $j$th subsection is given by

$$G_j(t) = \exp\left(\frac{\Gamma g_j(t)}{(1+\epsilon S_j)} - \alpha\right) L. \tag{6}$$

In (6), $\Gamma$, $g_j$, $\epsilon$, $S_j$, $L_j$, and $a$ are the confinement factor, material gain, nonlinear gain compression factor, average photon density, length, and loss coefficient inside the subsection, respectively. Carrier density is determined by solving the rate equation in each subsection using fourth-order Runge–Kutta method. The simulation parameters are provided in Table I.

In case of the NPS, in order to take in account the birefringence of the SOA, we adopted the same model approach as described in [12]. The active length of the SOA is divided into four equal subsections to realize the ASE noise and photon density distribution along the length of the amplifier. The incoming optical field propagating in $+z$ direction is decomposed into TE and TM modes. The material gains inside the $j$th section for the

TABLE II
SOA PARAMETERS USED IN NPS SIMULATIONS

| Parameter | Value |
|---|---|
| Active Volume | $800 \times 1.6 \times 0.2\ \mu m^3$ |
| Confinement Factor ($TE/TM$) | 0.2/0.14 |
| Linewidth Enhancement Factor ($TE/TM$) | 4/4 |
| Carrier Liftime | 500 ps |
| Material Gain Coefficient ($TE/TM$) | $2.75 \times 10^{-20}$/ $2.55 \times 10^{-20}$ $m^2$ |
| Carrier Density at Transparency | $10^{24}\ m^{-3}$ |
| Group Velocity | $10^8$ m/s |
| Loss in Active Layer ($TE/TM$) | $2700\ m^{-1}$ |
| Nonlinear Gain Compression Factor | $4.5 \times 10^{-23}\ m^3$ |
| Population Imbalance factor | 0.4 |

two modes are given by

$$g_j^{\mathrm{TE}}(t) = a^{\mathrm{TE}}(2N_{j,\mathrm{TE}}(z,t) + N_{j,\mathrm{TM}}(z,t) - N_0) \quad (7)$$

$$g_j^{\mathrm{TM}}(t) = a^{\mathrm{TM}}(2N_{j,\mathrm{TM}}(z,t) + N_{j,\mathrm{TE}}(z,t) - N_0) \quad (8)$$

where, $a^{\mathrm{TE}}$ and $a^{\mathrm{TM}}$ are the TE and TMdifferential gain coefficients, $N_{j,\mathrm{TE}}(z,t)$ and $N_{j,\mathrm{TM}}(z,t)$ are the hole densities involved in TE and TM transitions, and $N_0$ is the total electron density at transparency. Here, the contribution from the ultrafast intraband dynamics is neglected and equal spontaneous emission rates for both modes are assumed. This approach is found to describe well signal dynamics that occur on time scales corresponding to few gigahertz [12]. At equilibrium, $N_{j,\mathrm{TE}}(z,t)$ and $N_{j,\mathrm{TM}}(z,t)$ are assumed to be clamped together by population imbalance factor $f$, i.e.,

$$N_{j,\mathrm{TE}}(z,t) = fN_{j,\mathrm{TM}}(z,t). \quad (9)$$

We did not consider different group velocities for TE and TM modes as the active length was not long enough to produce any dispersion-induced distortion [17]. The line-width enhancement factor is assumed to be constant over a wide range of input power. This assumption remains valid as the SOA length and operating wavelength are kept fixed, and small variations in bias current are assumed [15]. The simulation parameters are summarized in Table II. The SOA parameters are chosen to match between SOA characteristics as obtained by simulation and experiment (the matching of the transfer function as well as the experimental setup is shown in Fig. 4). In the experiment, a variable continuous wave (CW) power (light at 1550 nm wavelength) was used as input. The CW was coupled with a $45^\circ$ angle in respect to the SOA axes. The output power was measured after an optical bandpass filter (OBPF, BW = 0.8 nm), which was used for the ASE noise rejection. The experiment and the simulations both resulted into 23 dB fiber-to-fiber small signal gain, 9 dBm output saturation power at 200 mA bias current and 0.5 dB polarization-dependent gain. The coupling loss was assumed to be 5 dB. In the simulations, the gains were estimated based on the linear relationship between material gain and carrier density, thus the assumed SOA parameters in the NPS only remain valid for a small range of bias current [12]. In the following we shall keep the SOA bias current at 200 mA for all numerical simulations of NPS.

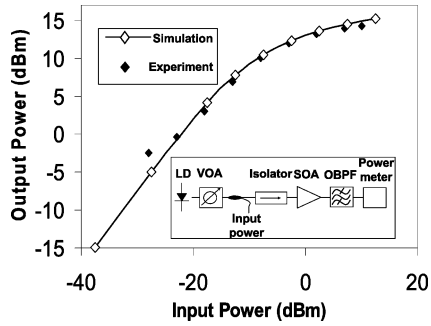


Fig. 4. Validation of the numerical model. Input Output characteristics of the SOA with 200 mA bias current. Inset shows the experimental setup. LD: laser diode. VOA: variable optical attenuator. OBPF: optical BPF (see text for SOA parameter details).

We note that this model reduces to the one adopted for the polarization insensitive SOA provided that birefringence is set to zero (i.e., the TE and TM gains are equal and the imbalance factor is set to 1). In this case, (7) and (7-8) reduce to (5) [18]. However, we used two different models for computational efficiency [only (5) must be solved in the case of polarization insensitive SOAs]. With SOA parameters adopted in our simulations, the SOAs had a recovery time of 450 ps for 200 mA bias current.

## IV. EQUIVALENCE OF THE SWITCHES

In this section, we investigate the equivalence of the two switches by numerical analysis, and derive the conditions in which such equivalence holds. We first discuss the functional equivalence in order to validate the equivalent model of the NPS introduced in Section II. For the sake of simplicity, we assumed a linearly polarized CW signal at the input (wavelength 1550 nm). To perform a direct comparison, in our simulations, we always set $x = a$. By doing this, both the switches had the same power imbalance at the input. For example, in order to compare an SOA–MZI with an input split ratio $x = 0.97$, we set the input PC in the NPS in order to have $\theta_{\mathrm{in}} = 10^\circ$ that gives $a = 0.97\,[\cos^2(10^\circ) = 0.97]$. Also, having fixed the bias current at 200 mA for all the SOAs (see Section III), we note that each amplifier had an input saturation power $P_{\mathrm{sat}}$ of $-14.5$ dBm. By setting $x = a = 0.97$ and $P_{\mathrm{in}} = 0.3P_{\mathrm{sat}}$ in order to operate in the linear regime, we found that the gain differences between the two orthogonal modes in the NPS and between $G_1$ and $G_2$ in the SOA–MZI were very close (1.2 and 1.1 dB, respectively). In the linear regime, there is a weak coupling between the NPS propagation modes, thus we expect that the absolute values of the gains ($G^{\mathrm{TE}}$ with $G_1$ and $G^{\mathrm{TM}}$ with $G_2$) to be also equal. We then analyzed the SOA gains of both switches as a function of the input power and the power coupling ratio $x$ (and $a$). The results are shown in Fig. 5.

In order to establish the functional equivalence of the NPS model (see Fig. 3) and the SOA–MZI, we compared $G^{\mathrm{TE}}$ to $G_1$

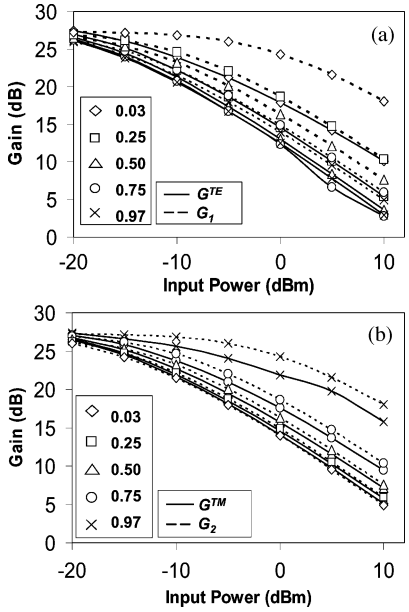


Fig. 5. Comparison of gains variation in NPS and SOA–MZI. (a) Variation of $G^{\mathrm{TE}}$ and $G_1$ against input power with $a$(or $x$) as parameter. (b) Variation of $G^{\mathrm{TM}}$ and $G_2$ against input power with $a$ (or $x$) as parameter.

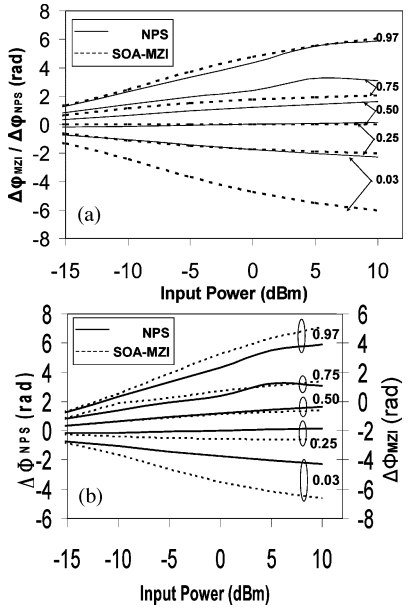


Fig. 6. Nonlinear phase difference in SOA–MZI and NPS as a function of switch input power. (a) All SOAs are biased at 200 mA current and power splitting ratios are taken as parameter. (b) SOA–MZI is biased with $I_1 = 200$ mA and $I_2 = 180$ mA. NPS is biased at 200 mA. Power splitting ratios are taken as parameter.

and $G^{\mathrm{TM}}$ to $G_2$. Fig 5(a) shows that the gain coefficients start to differ at increasing input powers. In particular, we observed that $G^{\mathrm{TE}}$ decreases more rapidly than $G_1$. However, this difference becomes large only for low $x$ (or $a$) values. On the contrary, for the same input power range, $G^{\mathrm{TM}}$ follows the $G_2$ compression at any $x$ value except for some small differences in the deep saturation regime, as illustrated in Fig. 5(b). This different behavior is due to the tensile strain in the SOA, which tends to reduce $G^{\mathrm{TE}}$ in favor of $G^{\mathrm{TM}}$ in the saturation regime [19]. Indeed, according to (7)–(9), the gain saturation of one mode in NPS forces the other mode to saturate as well. For low coupling ratio, when only a small fraction of the energy is coupled into the TE mode and the TM mode is strongly saturated; the saturation of $G^{\mathrm{TM}}$ also induces a strong gain compression in $G^{\mathrm{TE}}$. This behavior is not observed in SOA–MZI, which uses two independent SOAs. For example, when $a = x = 0.03$, we observe 9 and 16 dB of gain compression in $G_1$ and $G^{\mathrm{TE}}$, respectively, when the input power is changed from $-15$ to 10 dBm. However, the gain compressions of $G_1$ and $G^{\mathrm{TE}}$ measured for higher coupling ratios ($x = 0.97$) are very similar and differ by less than 2 dB over same the input power range [see Fig. 5(a), X symbol]. We then calculated the nonlinear phase differences by using (2) and (4) as a function of the input power and the power splitting ratio $x$ (and $a$). The results are shown in Fig. 6(a). As expected, the nonlinear phase variation in the switches is similar for high $x$ (or $a$) values. Indeed, this regime is the one in which the gain compression is comparable. For the lower power coupling ratios, the nonlinear phase differences acquire a large deviation. From Fig. 6(a), it is also possible to observe another intrinsic difference between the two switches: in balanced biasing conditions and for $x = 0.5$, the SOA–MZI is perfectly symmetric and $\Delta\phi_{\mathrm{MZI}}$ is constantly zero; while this is not possible in the NPS owing to the intrinsic asymmetric relationship between $G^{\mathrm{TE}}$ and $G^{\mathrm{TM}}$. However, it is interesting to note that $\Delta\phi_{\mathrm{NPS}}$ shows a flat zero response over the full input power range, for $a = 0.25$. In this case, the power imbalance is able to compensate for the intrinsic asymmetry. Moreover, while $\Delta\phi_{\mathrm{MZI}}$ is symmetric in respect to power imbalance [i.e., $\Delta\phi_{\mathrm{MZI}}(x) = \Delta\phi_{\mathrm{MZI}}(1-x)$], the tight coupling makes it impossible to observe such symmetry in $\Delta\phi_{\mathrm{NPS}}$.

Complete self-switching behavior can be obtained (in both switches) only when the input power variation results in a phase shift of $\pi$. Fig. 6(a) shows that while in the case of SOA–MZI, this is possible for high power imbalance factors (very high and very low power splitting ratios), in the case of NPS, this is possible only with a high coupling ratio $a$. However in this regime, as we discussed, the nonlinear phase variation and the individual gains are very similar in the two switches. It is important to enable the SOA–MZI device to behave like a self-switch even in the case of $x = 0.5$. This would allow for the use of commercial devices, most of which are designed with $x = 0.5$. This limit could be overcome by introducing an asymmetry in the bias currents, thus imposing different gain coefficients in the two arms of the SOA–MZI. In order to investigate the effect of bias current asymmetry in SOA–MZI, we then set $I_1 = 200$ mA and $I_2 = 180$ mA and compared the new $\Delta\phi_{\mathrm{MZI}}$ with $\Delta\phi_{\mathrm{NPS}}$ obtained previously [see Fig. 6(b)]. This imbalanced biasing in SOA–MZI has two major effects. First, $\Delta\phi_{\mathrm{MZI}}$ is no longer symmetric in respect to the power imbalance [i.e., now $\Delta\phi_{\mathrm{MZI}}(x) \neq \Delta\phi_{\mathrm{MZI}}(1-x)$]; and it introduces an offset of $\approx 2.0$ rad. Apart from this offset, the two nonlinear differential phases now show a common trend for any input splitting ratio. This indicates that for a fixed power splitting ratio, the imbalance of the bias currents induces an asymmetry in $G_1$ and $G_2$ that is very similar to the asymmetry in $G^{\mathrm{TE}}$ and $G^{\mathrm{TM}}$. Figs. 5 and 6 thus indicate the same functional equivalence of input PC

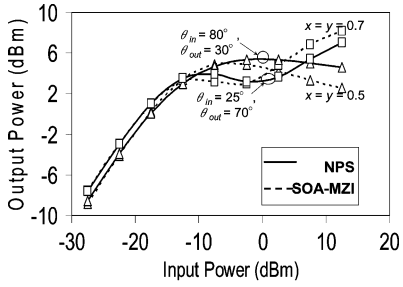


Fig. 7. Power transmission curve of NPS and SOA–MZI as obtained by numerical simulations for different power coupling ratios.

and the input power splitter in the two switches in determining similar gain and nonlinear phase difference as a function of switch input power under proper biasing conditions. The results also confirm the identical role of different light paths in SOA–MZI with the TE and TM modes in the NPS. This validates the functional equivalence of our interferometric model of NPS similar to SOA–MZI.

The next study was carried out to show the operational equivalence of the two switches in terms of their power transfer functions. The transfer functions are not merely determined by the differential gain; indeed, looking at (1) and (3), they also depend on the output splitting ratio (in the case of the NPS, the output splitting ratio is determined by the PBS and the PC, see Fig. 3). We have then compared the transmission curves of an NPS (biased at 200 mA) and an SOA–MZI with imbalanced driving currents ($I_1 = 200$ mA and $I_2 = 180$ mA as indicated previously). The SOA–MZI is assumed to have identical input and output coupling ratios (i.e., $x = y$). We have investigated two cases having symmetric ($x = 0.5$) and asymmetric ($x = 0.7$) power splitting. Then, we look for all possible input/output PC settings in the NPS that produce similar transfer functions as that of SOA–MZI. The power transfer characteristics of NPS for optimal pairs of $\theta_{\rm in}$ and $\theta_{\rm out}$ along with the SOA–MZI transmission curves are reported in Fig. 7. We highlight that Fig. 7 is drawn using detailed numerical simulation of the power transfer function for the SOA–MZI and NPS by considering both gain and nonlinear phases using (2) and (4).

The results show a common trend in the transmission characteristics for both the devices especially at low input power. Also in this case, as seen in Figs. 5 and 6, we observe a mismatch in the power transfer functions of the two switches at high input powers: the maximum output power difference is 2dB and it is observed at input power of 12.5 dBm (well above the output saturation power of the amplifier). The similarity in transfer characteristics of the switches indeed shows an operational equivalence between them. In this study, the optimal pairs of $\theta_{\rm in}$ and $\theta_{\rm out}$ are determined after many simulation runs, thus a more systematic approach in matching the transmission curves is needed. From the previous theoretical analysis and numerical simulations, we observed that the transfer functions of the switches are critically dependent on a number of different parameters, namely, the power coupling ratios, the bias currents, the amplifier gains, and nonlinear phase differences. Hence, it

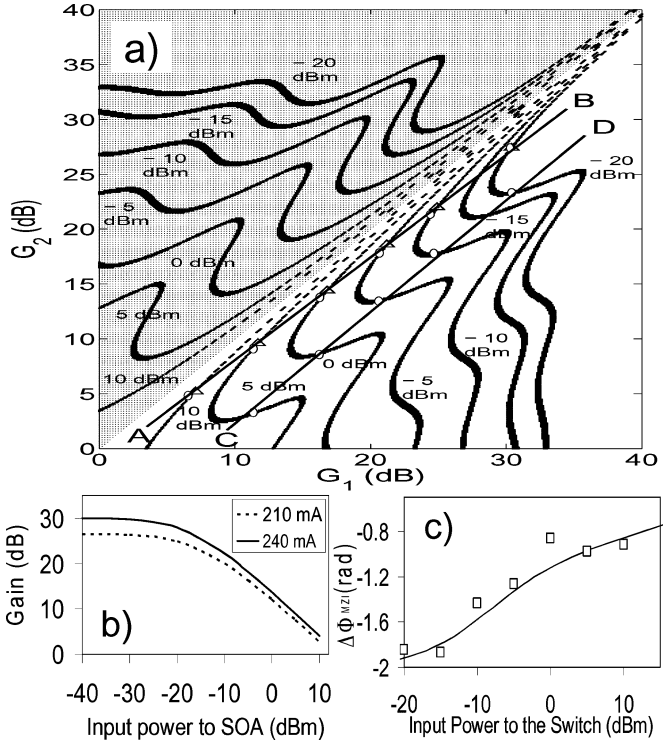


Fig. 8. (a) Graph shows all the possible gain combinations of the upper and lower arm SOAs in MZI switch that guarantee an identical power transfer function of an NPS; each curve is obtained for a specific input power level. (b) $G_1(P_{\rm in})$ and $G_2(P_{\rm in})$ variation calculated for $I_1 = 240$ mA and $I_2 = 210$ mA. (c) Comparison of ideal nonlinear phase difference in SOA–MZI (as evaluated through the gain combination curve and shown by open symbol) and the one obtained with the chosen combination (solid line).

is not easy to find a direct comparison between the two configurations. For this reason, we developed an approach to determine the operating conditions in which the switches produce closely matched input–output power transfer functions. The method consists of fixing an NPS configuration and deriving its modal gain $G^{\rm TE}$ and $G^{\rm TM}$, from those results, we determine the power coupling ratios and the bias imbalance of an SOA–MZI that give similar transmission curves. We illustrate this method with the aid of an example. For the sake of the simplicity, we consider an NPS and an SOA–MZI that have identical power splitting ratios (i.e., $x = a = y = b = 0.5$). We set the SOA bias current in the NPS at 200 mA. Then, we calculate the modal gains $G^{\rm TE}$ and $G^{\rm TM}$ (in this case, same as in Fig. 5). We then calculate which gain pair $[G_1, G_2]$ gives the same output power in the SOA–MZI as that of the NPS for a given input power level. To do this, we equate (1) with (3) and solve numerically for $[G_1, G_2]$ by using the $G^{\rm TE}$ and $G^{\rm TM}$ that we have determined.[1] From this calculation, we obtain a set of valid $[G_1, G_2]$ pairs at varying input power levels. In this way, we derive a numerical function that expresses the relation between $G_1$ and $G_2$ that is equivalent to the NPS. The plot of the function $G_2 = f(G_1)$ at varying input power to the switch is reported in Fig. 8(a). We refer this as "gain combination curves" of the SOA–MZI switch.

[1]The nonlinear phase differences are calculated by using (2) and (4).

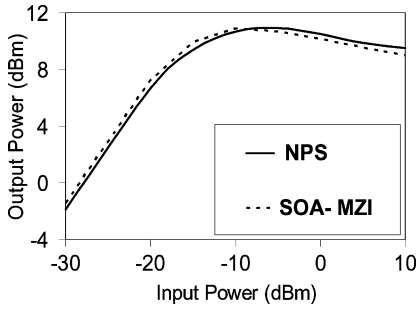


Fig. 9. Power transfer function of NPS and SOA–MZI device with the switch configurations calculated by using the gain combination curves.

The relation between $G_1$ and $G_2$ depends only on the NPS characteristics and is the one that gives the proper nonlinear phase shift to have similar self-switching as the NPS. By using the graph in Fig. 8(a), we can then derive the gain versus input power curve that the SOAs in the MZI [i.e., $G_1(P_{\rm in})$ and $G_1(P_{\rm in})$] must have to obtain a similar output trend. For example, it is possible to extrapolate the gain curve that the second SOA in the MZI must have once the other one is known or fixed. If for the sake of simplicity, we use for SOA1 known parameters (at a given current), we can locate its $G_1(P_{\rm in})$ curve over the gain combination curve of Fig. 8(a). Owing to the non-biunique shape of the curve, we can obtain one (or more) curve(s) corresponding to the same $G_1(P_{\rm in})$. As an example in Fig. 8(a), the lines $AB$ and $CD$ represent two smooth curves obtained by locating the points of the $G_1(P_{\rm in})$ curve for SOA1 biased at 240 mA [see circles in Fig. 8(a)]. Once these curves are obtained, it is possible to derive the $G_2(P_{\rm in})$ gain curve by extrapolating the corresponding points on the $G_2$ axis. In this case, starting from one gain saturation characteristic for SOA1, we were able to determine two possible gain saturation characteristics for SOA2 that ensures that the two transfer functions match over an input power variation ranging from $-20$ to 5 dBm. Note that we restricted our analysis to the case $G_1 > G_2$, i.e., within the unshaded region of Fig. 8(a). In most cases, the required $G_2(P_{\rm in})$ function can be obtained by simply choosing a proper bias current $I_2$. As in the present example, the choice of $I_2 = 210$ mA gives the values of $G_2(P_{\rm in})$ that correspond to the $AB$ line [see triangles in Fig. 8(a)]. The assumed $G_1$ curve (solid) and the extrapolated $G_2$ curve (dashed) are reported in Fig. 8(b). Fig. 8(c) reports the ideal nonlinear phase difference in the SOA–MZI switch as obtained from the gain combination curves near $AB$ line (open symbols); as a comparison, we also report (solid line) the nonlinear phase difference that corresponds to the bias currents combination that has been determined. As it can be seen, the nonlinear phase behavior approaches the optimal one. Indeed, by using the corresponding currents $I_1$ and $I_2$, we obtain a very good match between the transfer curves of the two switches, as reported in Fig. 9. Such high degree of matching has been obtained by simulating several different switches configurations, and it not related to a specific choice of the parameters. As discussed previously, we still found a mismatch between the curves in the deep saturation regime; however, we can see that by using the gain combination curves method, the mismatch (0.6 dB maximum) is highly reduced in respect to the 2 dB as found by successive trials method (see Fig. 7). By using the trial method, the input/output PCs were varied while keeping the bias currents of the two switches fixed. The mismatch (maximum 2 dB) between the transmission curves was due to nonoptimal choice of current pair $[I_1, I_2]$ in SOA–MZI switch. On the other hand, while estimating the transfer curves shown in Fig. 9, we had the prior knowledge of the gain saturation characteristics of SOA1 and SOA2 for a specific NPS configuration from the gain combination curves. This knowledge enabled us to choose proper bias current pair $[I_1, I_2]$ resulting a better match between the transmission curves of the two switches. We also note that similarity between the transfer functions can also be achieved using different $G_2(P_{\rm in})$ values extrapolated in correspondence of the other $CD$ line. Summarizing, the NPS and SOA–MZI behave equivalently from the transfer function point of view, when the operating conditions of the two switches are related with the gain combination curves shown in Fig. 8(a). We note that the curves in Fig. 8(a) have a finite thickness. This is due to the fact in their derivation, we equate (1) and (3) so that the output power levels difference ($\Delta P$) is less than 0.2 dB. The curves thickness might be reduced to zero by imposing $\Delta P = 0$. However, in practical implementations, the parameters used in the method, the set of coupling ratios $(a, b, x, y)$ and NPS bias current, are known with an experimental uncertainty that is taken in account by imposing $\Delta P \neq 0$. Of course, a radical change in the switches configurations would require a recalculation of the gain combination curve to obtain a good match.

## V. Experimental Validation

In the previous section, we discussed how to obtain an equivalent switching behavior of SOA–MZI and NPS. In this section, we extend our results and report an experimental characterization of such equivalence. In the following, we demonstrate that both devices can be operated as an all-optical power equalizer with very similar equalization ranges when properly biased. The use of an NPS switch as a power equalizer has been previously demonstrated [11]. On the other end, because the NPS is intrinsically polarization sensitive, it is not suitable to be used in front of an optical receiver. In this section, we first show experimentally that a 50% coupled SOA–MZI can provide power equalization in a 13 dB power range removing the polarization issue, and then, we derive how to set an NPS switch to obtain an equivalent power transfer function.

The experimental setup for realizing SOA–MZI-based power equalizer is shown in the inset of Fig. 10. We used a commercially available hybrid-integrated SOA–MZI device with 50% input/output power splitters/couplers. The device structure is depicted in the inset of Fig. 10. The SOAs in the device had around 27 dB small signal gain when biased at 300 mA. The single SOA gains are estimated by using the optical paths that allow the light to propagate in each single SOA (for example, referring to the inset of Fig. 10, by entering through port A and reading the gain at port H) and incorporating about 7 dB of total loss (comprising the low-losses internal couplers and the insertion losses of the device). The optical paths inside the SOA–MZI

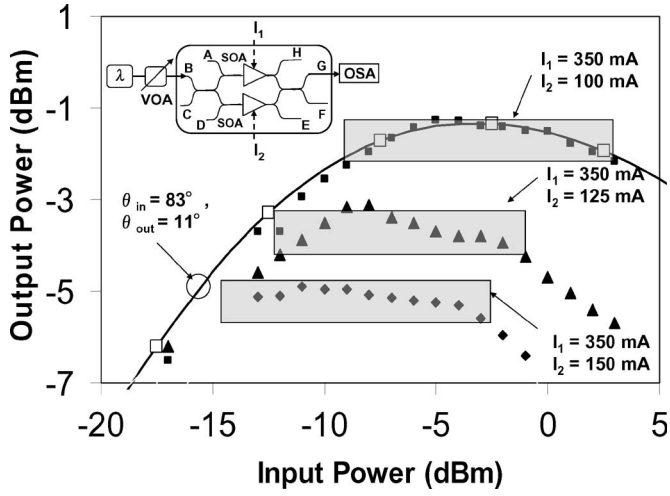


Fig. 10. Power equalization by SOA–MZI at different bias current settings obtained from experiment (closed symbols). Shadow boxes indicate the equalization ranges. The transfer curves of the self-NPS output as obtained from simulations (solid line with open symbols). Inset shows the experimental setup for power equalization using SOA–MZI switch. VOA: variable optical attenuator. OSA: optical spectrum analyzer.

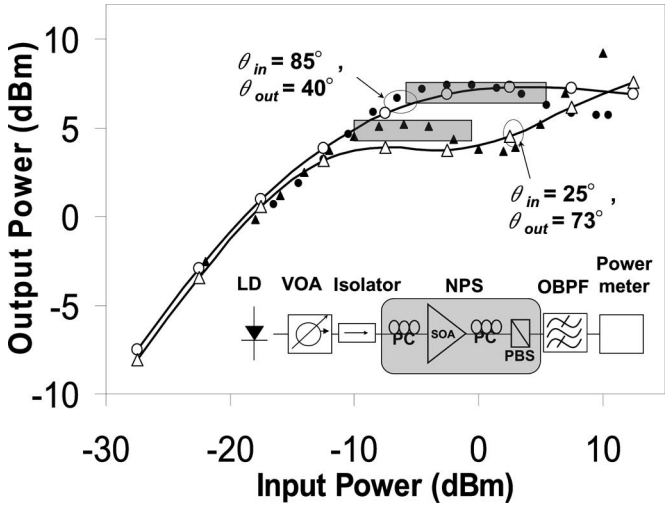


Fig. 11. Power equalization characteristics of the NPS as obtained from experiment (closed symbols) and from simulations (solid line with open symbols). Boxes show the equalization range obtained experimentally. Experimental setup shown within inset. LD: laser diode. VOA: variable optical attenuator. PC: polarization controller. OBPF: optical BPF.

device were balanced by using the internal thermooptic phase shifters. We then varied only the SOAs bias currents and the input optical power. The $1550$ nm input CW was launched into one port of the SOA–MZI device (port B). The output power was measured at the switched port by using a calibrated optical spectrum analyzer with a resolution set to $0.1$ nm; by doing this, we are able to read the effective signal power and isolate the outband ASE noise contributions at low output power levels. The power transfer function was measured over a wide range of input power levels (from $-20$ to $5$ dBm) for various values of bias currents. As we are interested in the strong bias imbalance regime, we kept one bias current ($I_1$) fixed at $350$ mA while changing the other one ($I_2$) from $150$ to $100$ mA. When the SOA–MZI device is operated in such a strongly bias imbalanced mode, it is possible to observe (Fig. 10) a region in which the transfer function is flat, i.e., in which the output power variation is confined in a $1$ dB interval. We define this region as the "equalization range" and it is measured to be about $13$ dB (from $-9$ to $4$ dBm input power) for the case in which $I_2$ is set to $100$ mA. By using the method illustrated in Section IV in reverse, we found a configuration in which an NPS switch would yield the same power transfer function.[2] Such a power transfer function is indicated by the continuous line in Fig. 10. By further increasing the $I_2$ value (to $125$ and $150$ mA), we observed that the overall output power is decreased. The important result is that the equalization range is kept roughly constant (around $13$ dB) and shifted toward lower input power levels. In the lower bias case, the equalization range is between $-15$ and $-2$ dBm input power, demonstrating that the power equalizer can operate successfully even at a low-power input signal. This is very important when the power equalizer is placed at the receiver side. The importance of this result is also found in the fact that this equalization range has been obtained for the first time with an SOA–MZI device with $50\%$ power coupling ratio (it was previously demonstrated experimentally only with a dedicated $70\%$ power split device [9]). We then performed an experimental characterization of the NPS as power equalizer. In this case, we used a commercial SOA biased at $200$ mA, resulting in $23$ dB small signal gain and $9$ dBm output saturation power. The output PBS had about $30$ dB extinction ratio. We measured the NPS static transfer function over the same wide input power range (from $-22$ to $10$ dBm) as in the case of the SOA–MZI. The NPS symmetry was varied by changing the input/output PC settings. We note that, in this case, it was not possible to measure experimentally the input and output polarization angles. However, we can estimate such values by numerical simulations after the measurements of the transfer functions.

In Fig. 11, we report two transfer functions corresponding to two selected input/output PC settings for which we obtained equalization ranges similar to those obtained in the case of the SOA–MZI. In particular, we obtained a configuration that results in a $13$ dB equalization range (from $-8$ to $5$ dBm input power, corresponding to $\theta_{\rm in} = 25^\circ$ and $\theta_{\rm out} = 73^\circ$). We note that this equalization range is very close to the one obtained experimentally with the SOA–MZI (in the case of $350$ and $100$ mA biasing condition). The other configuration corresponds to the values $\theta_{\rm in} = 85^\circ$ and $\theta_{\rm out} = 40^\circ$, and it is reported in Fig. 11. It provides an $11$ dB equalization range (from $-12$ to $-1$ dBm) similar to the one obtained when the SOA–MZI was biased at $350$ and $150$ mA (although in the case of the NPS, the equalization range is lower by $2$ dB). This result confirms that the two switches can be used as power equalizing devices with very similar specifications.

To complete our analysis, we also studied by numerical simulations which degree of control is required on the NPS input

[2]This result has been derived numerically by simulating an NPS device that employs an SOA with the same gain saturation curve as the one of the SOAs placed in the MZI.

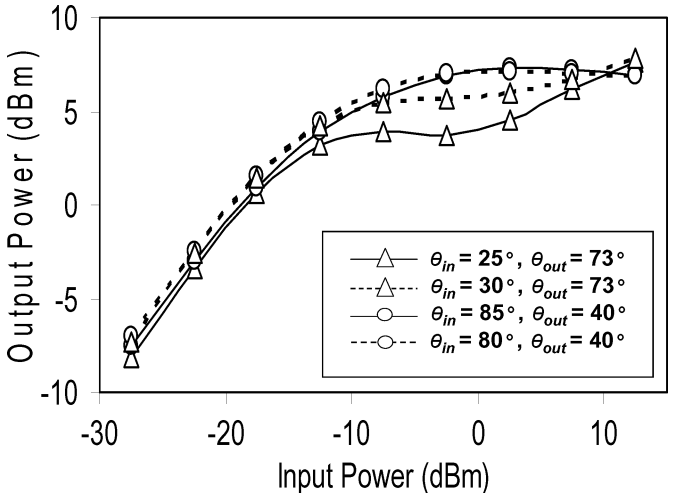


Fig. 12. Sensitivity of NPS transmission curves in respect to the input polarization angle. The solid curves correspond to the optimum settings as depicted in Fig. 11. The dashed curves are obtained for $\theta_{\rm in}$ differing by $5^\circ$ from the optimum values.

polarization angle in order to maintain the desired matching. We report in Fig. 12 a plot showing how the NPS transfer functions corresponding to the configurations reported in Fig. 11 vary when the input polarization angle is increased by $5^\circ$. We observed that the the configuration with $\theta_{\rm in} = 85^\circ$ is almost unaffected, while the configuration corresponding to $\theta_{\rm in} = 25^\circ$ is affected more significantly: indeed, in this case, the transfer function shows up to $2.5$ dB of difference, measured around $0$ dBm input power. Such maximum difference drops down to $1$ dB for input polarization angle variations lower than $2^\circ$. This value indicates the level of confidence at which the input polarization angle should be determined. The same behavior is observed for the situation reported in Fig. 7.

From the experimental characterization, the SOA–MZI and the NPS are found to provide power equalization over similar dynamic ranges, thus establishing the operational equivalence of these two devices. Owing to a limited amount of available information about the commercial SOA–MZI device, it was not possible to find two experimental configurations in which the static transfer characteristics of the switches exactly match, as predicted in Section IV. We also note that in the numerical analysis of Section IV, all the SOA have the same saturation characteristics (and same physical parameters). The experimental analysis has, however, been conducted with completely different devices. Notwithstanding these different devices, we found two experimental configurations where the match is close, allowing us to demonstrate experimentally their operational equivalence.

## VI. Conclusion

In this paper, we investigated the equivalence of the SOA–MZI and NPS when used as self-switches. Numerical simulation and experiment both show that a functional equivalence exists between the different components of the two switches. The input/output couplers in the SOA–MZI are equivalent with the input/output PCs in the NPS and the same role of the two separate SOAs in the MZI is played by the TE/TM modes in the NPS. We then show that an equivalent interferometric model of the NPS resembles the SOA–MZI device. The conditions of the switches for which both devices show similar gain and nonlinear phase difference are also discussed. We find that similar power transfer function for both the switches can be obtained under proper biasing conditions and with suitable power splitting ratios.

In order to find the configurations that match the power transfer functions of both the devices, we present an empirical method to determine the equivalent switching conditions. Simulation confirmed that this method can produce well-matched ($<0.6$ dB difference) power transmission curves over a wide range of input powers. Finally, we demonstrate experimentally the operational equivalence of both devices when operated as all-optical power equalizers. We observe power equalization of the SOA–MZI and the NPS over almost the same range of input power levels ($13$ dB). Moreover, we showed that the NPS model can be used to predict the power transfer characteristics that matches with the experimental results for both the switches. This theoretical and experimental study demonstrates that under certain regions of equivalence, the two switches can be interchanged showing practically the same input–output transfer power transfer characteristic.

## References

[1] K. Junya, H. Uenohara, and K. Kobayashi, "All-optical time domain label separation by SOA-MZI self-switching scheme," in *Proc. Soc. Conf. IEICE*, 2006, no. 2, p. 293.

[2] E. Patent, J. van der Tol, Y. Oei, M. Smit, M. Nielsen, J. Mork, and J. Binsma, "Integrated SOA-MZI for pattern-effect-free amplification," *Electron. Lett.*, vol. 41, no. 9, pp. 549–551, 2005.

[3] J. van der Tol, H. de Waardt, and Y. Liu, "A Mach–Zehnder-interferometer-based low-loss combiner," *IEEE Photon. Technol. Lett.*, vol. 13, no. 11, pp. 1197–1199, Nov. 2001.

[4] N. Calabretta, Y. Liu, F. Huijskens, M. Hill, H. de Waardt, G. Khoe, and H. Dorren, "Optical signal processing based on self-induced polarization rotation in a semiconductor optical amplifier," *J. Lightw. Technol.*, vol. 22, no. 2, pp. 372–381, 2004.

[5] J. Olmos, I. Monroy, J. Turkiewicz, Y. Liu, and A. Koonen, "Self-controlled all-optical label and payload separator for variable length bursts in a time-serial IM/DPSK scheme," *IEEE Photon. Technol. Lett.*, vol. 17, no. 8, pp. 1692–1694, Aug. 2005.

[6] N. Calabretta, G. Contestabile, A. D'Errico, and E. Ciaramella, "All-optical label processing techniques for pure DPSK optical packets," *IEEE J. Sel. Topics Quantum Electron.*, vol. 12, no. 4, pp. 686–696, Jul./Aug. 2006.

[7] E. Patent, J. van der Tol, J. Binsma, Y. Oei, E. Bente, and M. Smit, "Self-switching in Mach–Zehnder interferometers with SOA phase shifters," *IEEE Photon. Technol. Lett.*, vol. 17, no. 11, pp. 2301–2303, Nov. 2005.

[8] C. Janz, B. Lavigne, F. Poingt, I. Guillemot, F. Gaborit, B. Dagens, D. Chiaroni, and M. Renaud, "Low-penalty 10 Gbit/s operation of polarization-insensitive Mach–Zehnder wavelength converters based on bulk-tensile active material," in *Tech. Dig. Opt. Fiber Commun. Conf. Exhibit (OFC 1998)*, pp. 101–102.

[9] G. Kanellos, N. Pleros, D. Petrantonakis, P. Zakynthinos, H. Avramopoulos, G. Maxwell, and A. Poustie, "40 Gb/s 2R burst mode receiver with a single integrated SOA-MZI switch," *Opt. Exp.*, vol. 15, no. 8, pp. 5043–5049, 2007.

[10] M. Zhao, J. De Merlier, G. Morthier, and R. Baets, "All-optical 2R regeneration based on polarization rotation in a linear optical amplifier," *IEEE Photon. Technol. Lett.*, vol. 15, no. 2, pp. 305–307, Feb. 2003.

[11] B. Gopalakrishnapillai, M. Premaratne, A. Nirmalathas, and C. Lim, "Power equalization using polarization rotation in semiconductor optical amplifiers," *IEEE Photon. Technol. Lett.*, vol. 17, no. 8, pp. 1695–1697, Aug. 2005.

[12] H. J. S. Dorren, D. Lenstra, Y. Liu, M. T. Hill, G. D. Khoe, "Nonlinear polarization rotation in semiconductor optical amplifiers: Theory and application to all-optical flip-flop memories," *IEEE J. Quantum Electron.*, vol. 39, no. 1, pp. 141–148, Jan. 2003.
[13] C. Henry, "Theory of the linewidth of semiconductor lasers," *IEEE J. Quantum Electron.*, vol. 18, no. 2, pp. 259–264, Feb. 1982.
[14] L. Occhi, L. Schares, and G. Guekos, "Phase modeling based on the/spl alpha/-factor in bulk semiconductor optical amplifiers," *IEEE J. Sel. Topics Quantum Electron.*, vol. 9, no. 3, pp. 788–797, May/Jun. 2003.
[15] J. Park, X. Li, and W. Huang, "Comparative study of mixed frequency-time-domain models of semiconductor laser optical amplifiers," *Proc. Inst. Electr. Eng. Optoelectron.*, vol. 152, no. 3, pp. 151–159, Jun. 2005.
[16] M. Connelly, "Wideband semiconductor optical amplifier steady-state numericalmodel," *IEEE J. Quantum Electron.*, vol. 37, no. 3, pp. 439–447, Mar. 2001.
[17] X. Yang, D. Lenstra, G. Khoe, and H. Dorren, "Nonlinear polarization rotation induced by ultrashort optical pulses in a semiconductor optical amplifier," *Opt. Commun.*, vol. 223, pp. 169–179, 2003.
[18] W. Wang, K. Allaart, and D. Lenstra, "Semiconductor optical amplifier gain anisotropy: Confinement factor against material gain," *Electron. Lett.*, vol. 40, no. 25, pp. 1602–1603, Dec. 2004.
[19] M. Connelly, "Wide-band steady-state numerical model and parameter extraction of a tensile-strained bulk semiconductor optical amplifier," *IEEE J. Quantum Electron.*, vol. 43, no. 1, pp. 47–56, Jan. 2007.

**Sumanta Gupta** was born in Dhanbad, India, in 1976. He received the B.Sc.(Hons.) degree in physics, the B.Tech. and M.Tech. degrees in radiophysics and electronics from Calcutta University, Kolkata, India, in 1998, 2001, and 2003, respectively. He is currently working toward the Ph.D. degree in the Department of Electronics and Electrical Communication Engineering, Indian Institute of Technology-Kharagpur, Kharagpur, India.

His current research interests include investigation of advanced modulation formats, equalization, performance monitoring, and all-optical signal processing in high-speed fiber-optic communication systems.

**Nicola Calabretta** received the B.S. and M.S. degrees in telecommunications engineering from the Politecnico di Torino, Turin, Italy, in 1995 and 1999, respectively, and the Ph.D. degree in optical communication from the Communication Technology Basic Research and Applications (COBRA) Research Institute, Eindhoven University of Technology, Eindhoven, The Netherlands, in 2004.

In 1999, he received a scholarship to carry out his Master's thesis at the Eindhoven University of Technology, where he investigated a novel cost-effective system for monitoring wavelength-division multiplexing channels. He was engaged in research on all-optical signal processing in nonlinear medium to achieve functionalities for all-optical packet-switched cross-connect nodes. He is currently a Researcher with the Scuola Superiore Sant'Anna University, Pisa, Italy. He is the author or coauthor of more than 35 papers published in international journals and conferences. His current research interests include all-optical signal processing for optical packet switching, semiconductor optical amplifiers, all-optical wavelength conversion and regeneration, and advanced modulation formats for optical packet switching.

Dr. Calabretta is the recipient of the KIWI Telecom Awards 2004, Schipool, The Netherlands, for the innovative content reported in his Ph.D. thesis.

**Marco Presi** was born in Rome, Italy, in 1975. He received the Laurea degree in physics from the "La Sapienza" University, Rome, in 2001, and the Ph.D. degree in applied physics from Pisa University, Pisa, Italy.

In 2002, he joined the Optical System Group, Scuola Superiore Sant'Anna, Pisa. His current research interests include all-optical clock recovery, semiconductor optical amplifier, and passive optical networks.

**Giampiero Contestabile** received the Laurea degree in physics from the "La Sapienza" University of Rome, Rome, Italy, in 1998, and the Ph.D. degree in electrical engineering telecommunications from the "Tor Vergata" University of Rome, Rome, in 2001.

During 1996–2000, he was with the Semiconductor Devices Group, "Fondazione Ugo Bordoni", Rome. During 2000–2001, he was with the Optospeed Italia. Since September 2002, he has been an Assistant Professor at the Scuola Superiore Sant'Anna of University Studies and Doctoral Research of Pisa, Pisa, Italy. He coauthored more than 80 papers published in international journals and presented in leading international conferences. He is one of the reviewers of the *Journal of Lightwave Technology, Optics Express*, *Optics Letters, and Optics Communications*. His current research interests include advanced wavelength-division multiplexing (WDM) systems, optical packet switched networks, and applications of semiconductor optical amplifiers.

Dr. Contestabile is one of the reviewers of the IEEE PHOTONICS TECHNOLOGY LETTERS.

**Adrian Wonfor** (M'02) received the B.Sc. degree in physics from the University of Bath, Somerset, England U.K., in 1992.

He is a Senior Research Associate at the Centre for Photonic Systems, Engineering Department, University of Cambridge, Cambridge, U.K. His current research interests include network performance emulation, novel modulation schemes, high bit rate datacoms, radio over fiber, and optical access networks.

**Ranjan Gangopadhyay** (M'92) was born in Chandannagore, Hooghly, India, on September 10, 1944. He received the M.Tech. degree in radiophysics and electronics from Calcutta University, Kolkata, India, in 1966, and the Ph.D. degree digital communication from the Indian Institute of Technology (IIT)-Kharagpur, Kharagpur, India, in 1978.

During 1966–1980, he was a Lecturer in the Bengal Engineering College. In 1980, he joined the Department of Electronics and Electrical Communication Engineering, IIT-Kharagpur, as an Assistant Professor, and became a Professor in 1991, the Head of the Department during 2003–2005, and currently serves as an Emeritus Professor in the G. S. Sanyal School of Telecommunication. He also served as a Visiting Professor in the University of Parma, Italy, the Scuola Superiore Sant'Anna, Pisa, Italy, and in Chonbuk National University, Korea. His current research interests include telecommunication system engineering including optical networks, all-optical signal processing, and wireless communication.

**Ernesto Ciaramella** (M'06) was born in Rome, Italy, in 1967. He received the Laurea degree (*cum laude*) from the "La Sapienza University," Rome, in 1991.

In 1992, he received a scholarship from Alcatel. During 1992–1994, he was a Researcher with the "Fondazione Ugo Bordoni," where he was engaged in research on nonlinear optical effects. During 1994–1998, he was with the Centro Studie Laboratorie Telecommunicazioni S.p.A., Turin, Italy, where he was engaged in research on linear and nonlinear propagation effects in optical fibers, and then, with numerical modeling of high-capacity optical systems, and contributed to the CSELT-Telecom Italia Working Group on wavelength-division multiplexing systems. During 1998–2000, he was a Scientific Researcher with the "Fondazione Ugo Bordoni," where he was engaged in research on optical-transmission systems and network architectures. During 2001–2002, he was a Research Manager at the Consorzio Nazionale Interuniversitario per le Telecomunicazioni (CNIT) National Photonic Networks Laboratory, Pisa, Italy. Since 2002, he has been an Associate Professor with the Scuola Superiore Sant'Anna, Pisa. His current research interests include optical communications (components, systems, and networks). He participated in various European research projects, published approximately 90 papers, and is the author or coauthor of five international patents.